Sensors and Materials, Vol. 35, No. 12 (2023) 4417–4437
MYU Tokyo

S & M 3489

Low-carbon Economic Operation Optimization of Integrated Energy System Considering Carbon Emission Sensing Measurement System and Demand Response: An Improved Northern Goshawk Optimization Algorithm

Ling-ling Li,[1,2] Yan Miao,[1,2] Cheng-Jian Lin,[3*]
Linan Qu,[1,2] Guanchen Liu,[4] and Jianping Yuan[5]

[1]State Key Laboratory of Reliability and Intelligence of Electrical Equipment, Hebei University of Technology, Tianjin 300401, China
[2]Key Laboratory of Electromagnetic Field and Electrical Apparatus Reliability of Hebei Province, Hebei University of Technology, Tianjin 300401, China
[3]Department of Computer Science & Information Engineering, National Chin-Yi University of Technology, Taichung 411, Taiwan
[4]Power China Huadong Engineering Corporation Ltd., Hangzhou 310000, China
[5]Hangzhou Huachen Electric Power Control Co., Ltd., Hangzhou 310014, China

(Received July 12, 2023; accepted December 11, 2023)

Keywords: integrated electricity–heat energy system, improved northern goshawk algorithm, carbon emission sensing measurement system, demand response

The integrated energy system is a perfect way to realize the transformation of the traditional energy industry structure. To further explore the role of its load-side adjustable potential in carbon emission reduction, an optimal operation model of the integrated energy system considering the carbon emission sensing measurement system and demand response (DR) is proposed. First, the integrated electricity–heat energy system (IEHS) model framework is constructed in accordance with the coupling characteristics of electricity–heat–gas in the system. The carbon emission sensing measurement system is introduced on the energy supply side, and DR is considered on the user load side, including the DR model based on the price elasticity matrix and the replacement-based DR model considering the mutual conversion of electric and thermal energies on the energy use side. Second, the baseline method is used to allocate carbon emission quotas for the system free of charge, and the actual carbon emissions of gas turbines and gas boilers are considered. An IEHS objective function is established to minimize the sum of the energy purchase, carbon transaction, and operation and maintenance costs. Third, an improved northern goshawk optimization (INGO) algorithm is proposed to optimize the low-carbon operation of the IEHS model. Finally, the effectiveness and practicability of the proposed model and algorithm are verified using different scenarios and different algorithms. The results show that, considering the carbon emission sensing measurement system and DR, the total operation cost is reduced by 10.4% and the actual carbon emission is reduced by 6420.582 kg. Compared with those of the northern goshawk (NGO)

*Corresponding author: e-mail:cjlin@ncut.edu.tw
https://doi.org/10.18494/SAM4679

ISSN 0914-4935

algorithm, the total operation cost of the INGO algorithm is reduced by 9.4% and the actual carbon emission is reduced by 1164.253 kg, which realizes the coordinated operation of system economy and low carbon emission.

1. Introduction

The structure of the energy industry has gradually shifted to the high efficiency and environmental protection direction, showing two major characteristics of renewable energy access and diversified power load. The proposal of a "double carbon" target has brought new challenges to the energy and power industry and is the main force behind pollutant emission reduction. On the one hand, renewable energy, represented by photovoltaic (PV) and wind turbine (WT) energy, has developed rapidly, and the ratio of clean energy to primary energy has increased. However, the output of clean energy has the characteristics of randomness and uncertainty, which make the light curtailment and wind curtailment phenomena serious. The reasonable storage of residual energy is the key to dealing with these problems. On the other hand, in the context of building a novel type of system, the energy structure has undergone a major transformation.(1) With the advancement of energy conversion technology and the iterative innovation of conversion equipment, the barriers of multiple heterogeneous energy subsystems are gradually being overcome.(2) An integrated energy system can effectively solve the energy crisis, realize multi-energy coupling, and achieve the targets of carbon dioxide emission reduction.(3)

In the face of the current situation, the coupling relationship between a variety of energies and an integrated electricity–heat energy system (IEHS) needs to be further elucidated, and the carbon emissions of different equipment need to be reduced. The carbon emission sensing measurement system can not only improve resource allocation, but also enhance energy conversion and emission reduction.(4) If this mechanism is introduced in IEHS, it can make carbon emission rights (CERs) a schedulable resource with economic value. In addition, for the energy supply load demand sides in the IEHS model, the introduction of demand response (DR) can improve the two-way interaction between these sides. At present, most of literatures are analyzed from the aspect of maximizing the economic interests of IEHS and less consideration is given to energy conversion and pollutant emission,(5) and the conventional algorithm may lead to the lack of global search and optimization abilities in the multi-energy flow coupling operation of IEHS. Therefore, it is necessary to find an efficient and accurate solution method and apply it to the economic operation of IEHS multi-energy flow coupling.

Regarding the utilization of the carbon emission sensing measurement system and DR in IEHS, Zheng *et al.*(6) presented a particle swarm optimization (PSO) algorithm based on chaos to realize the optimal scheduling of the integrated energy system under the high volatility of renewable energy load. In contrast to the traditional PSO algorithm, the economic cost was increased by 3.868%, and the stability of the comprehensive operation was guaranteed. However,

the optimal scheduling of the integrated energy system only considers the economic cost and fails to consider the environmental benefits. Yao *et al.*[7] studied the dynamic capacity flow analysis model and method of the power and heat networks in an integrated energy system, and solved the high-dimensional discretization model through a decomposition-iteration algorithm, which simplified the model operation process and improved the calculation accuracy of energy flow. Aiming at the complex energy coupling and source-load uncertainty in integrated energy system dynamic scheduling, Xu and Xiang[8] proposed an optimal scheme in accordance with determination strategy gentrification algorithms and verified the stability and applicability of the algorithms. Deng *et al.*[9] constructed an integrated energy system effective scheduling model with wind and solar energy storage. The comprehensive operation cost was considered in the objective function, and an improved krill herd algorithm was utilized to optimize the dispatch model, which improved the energy utilization and economy. However, the objective function considered is relatively simple. In contrast to the original algorithm, the computational capabilities of the improved krill herd algorithm need to be further explored.

To reasonably solve the problems of IEHS operation optimization, we effectively reduce the general economic cost and carbon emission, and improve the evolution of the carbon economy and the permeation rate of new energy. Using the carbon emission sensing measurement system and DR, the IEHS low-carbon economic model is constructed. The improved northern goshawk optimization (INGO) algorithm is selected to obtain the optimal scheme for the optimization of the IEHS economic operation. The results of the model are also compared and analyzed for various scenarios. The main contributions are as follows.

1. A carbon emission sensing measurement system is considered in the IEHS model to increase the economic cost of IEHS and reduce the carbon emission of the system.
2. Price- and replacement-based DRs are considered on the load demand side. Consequently, the load fluctuation is stabilized and a stable operation of the IEHS low-carbon economy is realized.
3. An INGO algorithm is proposed to increase convergence speed and convergence accuracy, and enhance the optimization ability, and it is applied to the IEHS model, whereby the optimal dispatch solution is obtained.
4. A variety of cases with different scenarios of the same algorithm and different algorithms of the same scenario are compared to prove the effectiveness and practicality of the proposed IEHS model and INGO algorithm.

The remaining sections are organized as follows. In Sect. 2, we construct the IEHS model framework, including the energy-supply-side carbon emission sensing measurement system model and the user-load-side demand response model. In Sect. 3, we optimize the operation of the IEHS model, including the construction of the IEHS operation objective function and the proposal of an INGO algorithm. In Sect. 4, we use regional cases to analyze the optimization results of the IEHS low-carbon economic operation, and we provide the conclusions and future research directions.

2. Integrated Electricity–heat Energy System

2.1 Structure of IEHS

In this study, the IEHS model framework shown in Fig. 1 is constructed. Electric and gas energies are offered by a superior grid and a gas network, respectively, and natural gas is purchased for the combined heat and power (CHP) and auxiliary energy supply equipment gas boiler (GB). When the power is in excess or insufficient, it is sold to or purchased from the superior grid, respectively.[10] The energy coupling devices include PV, WT, CHP, GB, and heat pump (HP), where CHP includes a waste heat boiler (WHB), a gas turbine (GT), and the Organic Rankine Cycle (ORC) system and operates as a thermal-electrolytic decoupling system, whereas HP and GB consume the power produced by PV and WT and bear part of the thermal load. Owing to the volatility of PV and WT power generation, energy storage devices, including a battery (BAT) and a heat storage tank (HST), are added to IEHS to realize the time and space transfer of energy in different periods.[11] In addition, considering the DR strategy enables the smooth adjustment of the load profile for peak shaving and valley filling.[12] The structure of the IEHS model is shown in Fig. 1.[13–15]

2.2 Model of demand response

The DR characteristics are divided into two types: one based on the response of price changes and another based on the response of policy incentives.[16]

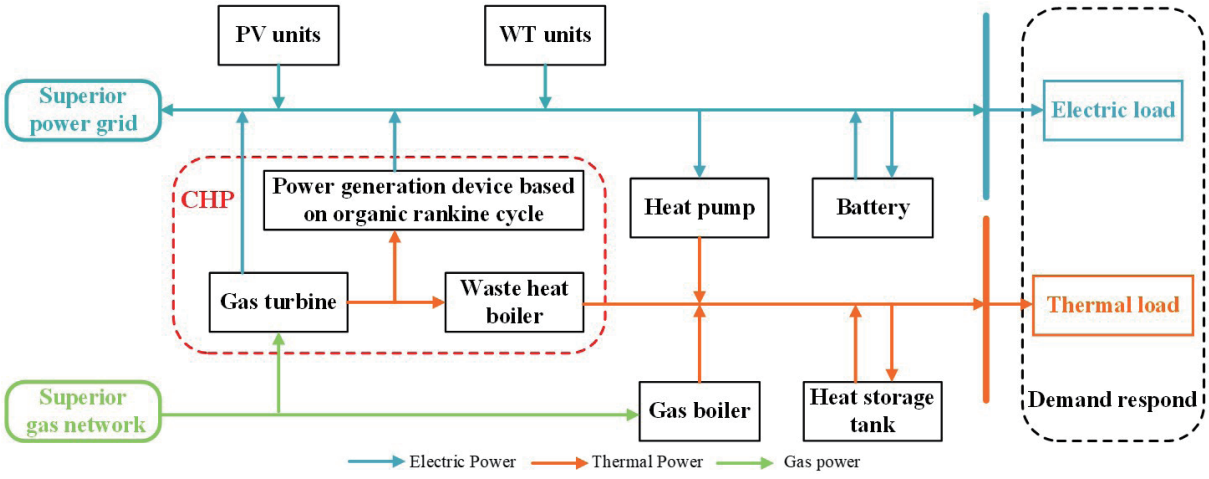

Fig. 1. (Color online) Diagram of IEHS frame structure.

2.2.1 Price-based DR

On the basis of the reasonable time-of-use electricity price, price-based DR guides users to change the behavior of electricity consumption independently and reduce or transfer the nonessential load.[17] Regarding the effect of price fluctuation, the users' electricity consumption behavior will also change to a certain extent. It is necessary to establish a price-based DR model of electricity load affected by price to determine the load transfer situation. The electricity price elasticity matrix effectively represents the sensitivity of users' electricity consumption to the time-of-use price, and it has the characteristics of wide use, accurate description, and strong evaluation. Therefore, in this study, we use the electricity price elasticity matrix to establish a model, as shown in

$$P_c(i,i) = \frac{\Delta P_i / P_i}{\Delta C_i / C_i}, \tag{1}$$

$$P_c(i,j) = \frac{\Delta P_i / P_i}{\Delta C_j / C_j}. \tag{2}$$

Here, $P_c(i, i)$ and $P_c(i, j)$ are self-elasticity and its coefficient, respectively. P_i and ΔP_i represent the amount of electrical load before DR and the amount of load change after DR at time i, respectively. C_i and ΔC_i represent the electricity prices before DR and after DR at time i, respectively. C_j and ΔC_j are the electricity prices before DR and after DR at time j, respectively.

The self-elasticity coefficient is the main diagonal element, the cross-elasticity coefficient represents other elements,[18] and the electricity price elasticity matrix is indicated as

$$\boldsymbol{PC} = \begin{bmatrix} P_{c,pp} & P_{c,pf} & P_{c,pl} \\ P_{c,fp} & P_{c,ff} & P_{c,fl} \\ P_{c,lp} & P_{c,lf} & P_{c,ll} \end{bmatrix}, \tag{3}$$

where p represents the peak period of load, f represents the trough period of load, and l represents the normal period of load. Therefore, the final established price-based DR model is

$$\begin{bmatrix} P_p \\ P_f \\ P_l \end{bmatrix} = \begin{bmatrix} P_{p,0} \\ P_{f,0} \\ P_{l,0} \end{bmatrix} + \begin{bmatrix} P_{p,0} & 0 & 0 \\ 0 & P_{f,0} & 0 \\ 0 & 0 & P_{l,0} \end{bmatrix} \cdot \boldsymbol{PC} \cdot \begin{bmatrix} \Delta c_p / c_{p,0} \\ \Delta c_f / c_{f,0} \\ \Delta c_l / c_{l,0} \end{bmatrix}. \tag{4}$$

Here, P_p, P_f, and P_l are the average loads of each period after the price-based DR, $P_{p,0}$, $P_{f,0}$, and $P_{l,0}$ are the average loads of each period before the price-based DR, Δc_p, Δc_f, and Δc_l represent the changes in electricity price in each period after DR, and $c_{p,0}$, $c_{f,0}$, and $c_{l,0}$ represent the electricity prices before the adoption of time-of-use electricity price, which can be regarded as unified prices.

The price-based DR load is divided into curtailable and shiftable loads, and two types of load are modeled separately as follows.

The mathematical model corresponding to the curtailable load after considering DR is

$$\Delta P_{CL}(t) = P_{CL,0} + M_{CL}. \tag{5}$$

Here, $\Delta P_{CL}(t)$ is the amount of variation of curtailable load after considering DR, $P_{CL,0}$ is the initial curtailable load, and M_{CL} is the electricity price elasticity matrix corresponding to the curtailable load.

The mathematical model corresponding to the shiftable load after considering DR is

$$\Delta P_{SL}(t) = P_{SL,0} + M_{SL}, \tag{6}$$

where $\Delta P_{SL}(t)$ is the amount of variation of shiftable load after considering DR, $P_{SL,0}$ is the initial shiftable load, and M_{SL} is the electricity price elasticity matrix corresponding to the shiftable load.

2.2.2 Replacement-based DR

The mathematical model corresponding to the replaceable load is

$$\Delta P_{RL}(t) = -\frac{\varepsilon_e \epsilon_e}{\varepsilon_h \epsilon_h} \Delta H_{RL}(t), \tag{7}$$

where $\Delta P_{RL}(t)$ and $\Delta H_{RL}(t)$ are the replaceable electric load and the corresponding replaced thermal load, respectively. ε_e and ε_h are the unit calorific values, and ϵ_e and ϵ_h are the energy utilization rates.

2.3 Model of carbon emission sensing measurement system

2.3.1 Model of free carbon emission quota

The carbon emission quota is allocated in accordance with the total equivalent calorific value, as shown below.

$$E_{CO2,0}(t)=\rho\left[H_{GT}(t)+\theta P_{GT}(t)+H_{GB}(t)\right] \tag{8}$$

Here, $E_{CO2,0}(t)$ is the carbon emission quota of the system, ρ is the carbon emission allocation of electricity in the region, which is taken to be 0.57 t/(MW·h), and θ is the conversion coefficient of electricity.

2.3.2 Model of carbon emission cost

The actual carbon emission in IEHS is the sum of GT and GB:

$$E_{CO2,a}(t)=\vartheta_{GT}\left[H_{GT}(t)+\theta P_{GT}(t)\right]+\vartheta_{GB}H_{GB}(t), \tag{9}$$

where $E_{CO2,\alpha}(t)$ is the actual carbon emission, and ϑ_{GT} and ϑ_{GB} are the carbon emission coefficients of GT and GB, respectively.

2.3.3 Model of stepped carbon emission trading

The amount of carbon emission trading is obtained as

$$E_{IEHS}(t)=E_{CO2,a}(t)-E_{CO2,0}(t), \tag{10}$$

where $E_{IEHS}(t)$ is the carbon emission trading volume of IEHS at time t.

The corresponding mathematical model is

$$C_{CO2}(t)=\begin{cases}\beta E_{IEHS}(t), & E_{IEHS}(t)\le\varphi\\ \beta(1+\tau)\left[E_{IEHS}(t)-\varphi\right]+\beta\varphi, & \varphi<E_{IEHS}(t)\le 2\varphi\\ \beta(1+2\tau)\left[E_{IEHS}(t)-2\varphi\right]+(2+\tau)\beta\varphi, & 2\varphi<E_{IEHS}(t)\le 3\varphi\\ \beta(1+3\tau)\left[E_{IEHS}(t)-3\varphi\right]+(3+3\tau)\beta\varphi, & 3\varphi<E_{IEHS}(t)\le 4\varphi\\ \beta(1+4\tau)\left[E_{IEHS}(t)-4\varphi\right]+(4+6\tau)\beta\varphi, & 4\varphi<E_{IEHS}(t)\end{cases}. \tag{11}$$

Here, $C_{CO2}(t)$ is the stepped carbon trading cost, β is the base price, φ is the interval length, and τ is the price growth rate.

3. IEHS Operation Optimization

On the basis of the above IEHS model, the objective function composed of three parts of cost and four constraints are constructed. In addition, the INGO algorithm is selected to solve the IEHS model to obtain the scheduling scheme.[19] The process of IEHS operation optimization is shown in Fig. 2.

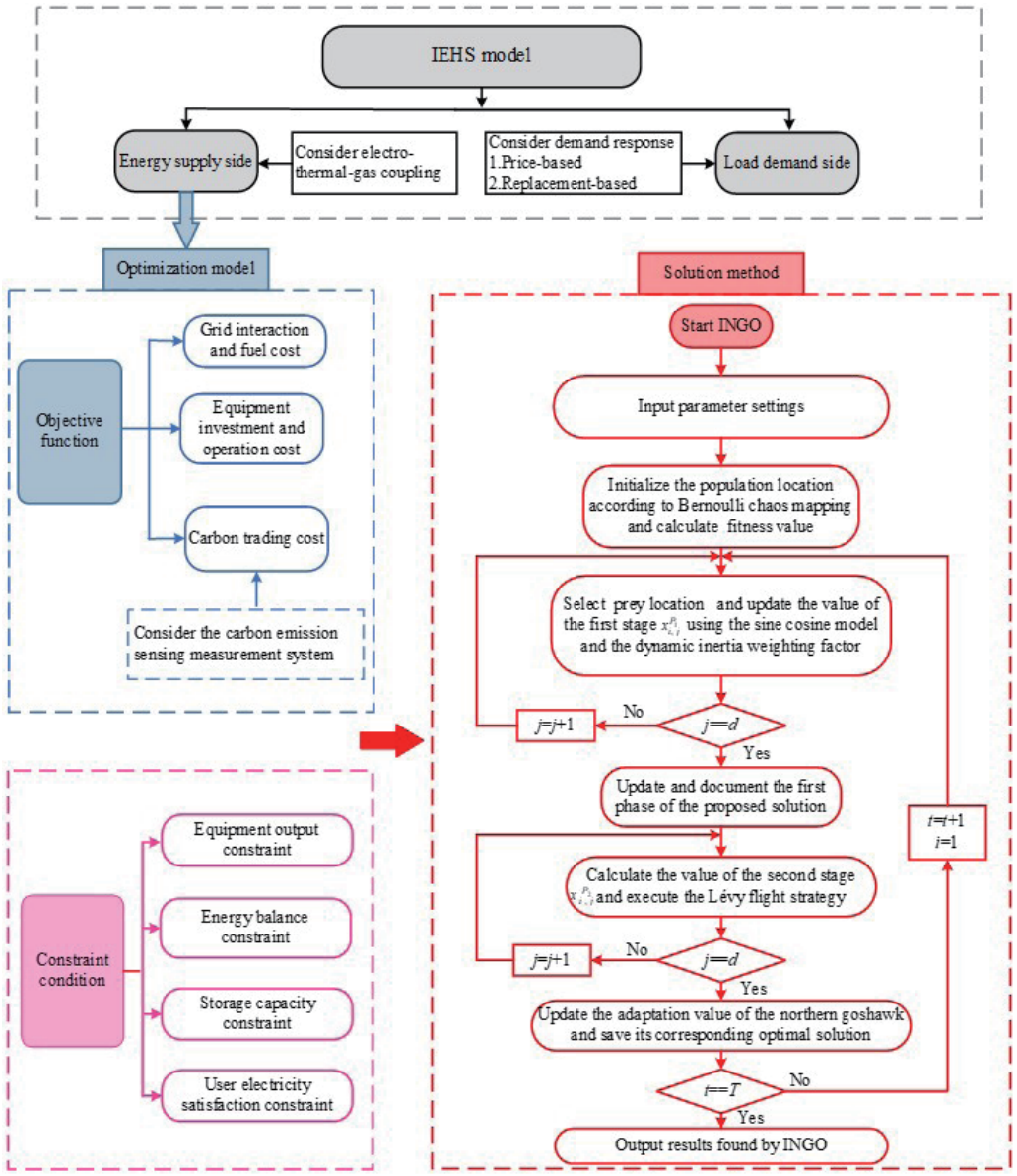

Fig. 2. (Color online) IEHS operation optimization diagram.

3.1 Objective function

Regarding the IEHS model, the authors consider the comprehensive operation cost to promote the optimization of the low-carbon economic operation of the system. In this study, a time of one day is selected as the research period, and the minimum sum of the power grid interaction and fuel cost, the carbon trading cost, and the equipment investment and operation cost are considered in the objective function to construct the following IEHS operation optimization model:

$$\min f = f_1 + f_2 + f_3. \tag{12}$$

Here, f is the total cost of the IEHS operation optimization, f_1 is the power grid interaction and fuel cost, f_2 is the carbon trading cost, and f_3 is the equipment investment and operation cost.

3.1.1 Power grid interaction and fuel cost

The cost of power grid interaction and fuel includes the cost of IEHS interaction with the power grid and the cost of fuel consumption. The mathematical model is

$$f_1 = C_{Grid} + C_{Fuel}, \tag{13}$$

$$\begin{cases} C_{Grid} = \sum_{t=1}^{T} k_{buy} P_{buy}(t) - \sum_{t=1}^{T} k_{sell} P_{sell}(t) \\ C_{Fuel} = \sum_{t=1}^{T} c_g G_{buy}(t) \end{cases}. \tag{14}$$

Here, C_{Grid} and C_{Fuel} are the cost of the IEHS interaction with the power grid and the cost of fuel consumption, respectively. T is the operation cycle, and k_{buy} and k_{sell} are the unit prices of electricity purchased and sold by the superior grid, respectively. $P_{buy}(t)$ and $P_{sell}(t)$ are the power purchase and power sales of IEHS, respectively. c_g is the natural gas price and $G_{buy}(t)$ is the total amount of gas purchased by IEHS.

3.1.2 Carbon trading cost

The carbon trading cost is the sum of all costs in an operating cycle, and the mathematical model is

$$f_2 = \sum_{t=1}^{T} C_{CO2}(t). \tag{15}$$

Here, $C_{CO2}(t)$ is the stepped carbon trading cost.

3.1.3 Equipment investment and operation cost

The mathematical model is

$$f_3 = C_{inv} + C_{ope}, \tag{16}$$

$$\begin{cases} C_{inv} = \mu(r,l)\sum_{i=1}^{N} c_i^{inv} x_i P_i / 365l, \\ C_{ope} = \mu(r,l)\sum_{i=1}^{N} c_i^{ope} x_i P_i / 365l. \end{cases} \tag{17}$$

Here, C_{inv} and C_{ope} are the investment and operation costs of the IEHS equipment, respectively. $\mu(r, l)$ is the depreciation coefficient, x_i is the number of type i equipment, P_i is the output power, N is the number of different equipment types, and c_i^{inv} and c_i^{ope} are the investment and operation costs of type i equipment, respectively.

3.2 Constraint condition

The energy balance constraints are shown as

$$\begin{aligned} &P_{buy}(t) - P_{sell}(t) + P_{PV}(t) + P_{WT}(t) + P_{GT}(t) + P_{ORC}(t) - P_{HP}(t) + E_{BAT,D}(t) - P_{BAT,C}(t) \\ &= P_{EL,0}(t) + \Delta P_{CL}(t) + \Delta P_{SL}(t) + \Delta P_{RL}(t), \end{aligned} \tag{18}$$

$$\begin{aligned} &H_{GT}(t) + H_{WHT}(t) + H_{HP}(t) + H_{GB}(t) + H_{HSD,D}(t) - H_{HSD,C}(t) \\ &= P_{HL,0}(t) + \Delta H_{RL}(t), \end{aligned} \tag{19}$$

$$G_{buy}(t) = G_{GT}(t) + G_{GB}(t). \tag{20}$$

Here, $P_{EL,0}(t)$ and $P_{HL,0}(t)$ are the electric and thermal loads at time t before considering DR, respectively.

3.3 Solution method

The swarm intelligence optimization algorithm is an algorithm that enhances the search ability of the solution space in a certain range by simulating the motion and behavior rules of some animals or things in nature and optimizing their target in a random manner. Such algorithms have attracted the research interest of scholars from various fields and countries. Particle swarm optimization (PSO), whale optimization algorithm (WOA), and ant lion optimization (ALO) have been proposed to solve various optimization problems in various fields.[20]

Dehghani *et al.*[21] was inspired by the behavior of northern goshawks capturing prey. In 2022, a novel intelligent optimization algorithm, the NGO algorithm, was proposed. Its principle is easy to understand, and it also has certain advantages in terms of the convergence speed of the

algorithm. However, there are some shortcomings in convergence accuracy; their final targets easily fall into a local optimum resulting in increased errors and deviation from the real results.[22] Therefore, in this paper, we improve the original NGO algorithm and verify its performance through test functions. The INGO algorithm is as follows.

3.3.1 Bernoulli chaotic mapping

The chaotic mapping formula is shown as

$$h_{w+1} = \begin{cases} h_w / (1-p), h_w \in (0, 1-p] \\ (h_w - 1 + p) / p, h_w \in (1-p, 1] \end{cases}, \tag{21}$$

where h_w is the chaotic value of w_{th} and p is the chaotic parameter.

3.3.2 Sine-cosine oscillation variation

The sine-cosine oscillation variation comes from the sine-cosine algorithm (SCA), and the objective function is repeatedly solved in accordance with the oscillation variation of the sine-cosine model. The sine-cosine oscillation variation is introduced in the first stage of the NGO algorithm, which improves the ability of global optimization and local search, and the corresponding mathematical model update formula after improvement is shown as

$$x_{i,j}^{P_1}(t+1) = \begin{cases} x_{i,j}^{P_1}(t) + \omega_1 \cdot \sin(\omega_2) \cdot \left| \omega_3 \cdot p_{i,j}(t) - x_{i,j}^{P_1}(t) \right|, F_{P_i} < F_i \\ x_{i,j}^{P_1}(t) + \omega_1 \cdot \cos(\omega_2) \cdot \left| \omega_3 \cdot p_{i,j}(t) - x_{i,j}^{P_1}(t) \right|, F_{P_i} \geq F_i, \end{cases} \tag{22}$$

$$\omega_1 = \left[1 - (t/T)^{\delta} \right]^{1/\delta}. \tag{23}$$

Here, ω_1 is the improved step search factor, δ is the adjustment coefficient with $\delta \geq 1$, $\omega_1 \in [0, 2\pi]$, which controls the moving distance of the northern goshawk, and $\omega_3 \in [0, 2]$, which controls the position update of the northern goshawk.

3.3.3 Dynamic inertia weighting factor

On the basis of Eq. (22), the dynamic inertia weighting factor is added to change the search mode of northern goshawks, thereby accelerating the speed of searching the global space.[23] The mathematical model corresponding to the dynamic inertia weighting factor is introduced as

$$x_{i,j}^{P_2}(t+1)=\begin{cases}\theta x_{i,j}^{P_1}(t)+\omega_1\cdot\sin(\omega_2)\cdot\left|\omega_3\cdot p_{i,j}(t)-x_{i,j}^{P_1}(t)\right|, F_{P_i}<F_i\\ \theta x_{i,j}^{P_1}(t)+\omega_1\cdot\cos(\omega_2)\cdot\left|\omega_3\cdot p_{i,j}(t)-x_{i,j}^{P_1}(t)\right|, F_{P_i}\geq F_i,\end{cases} \tag{24}$$

$$\theta=\left[\theta_1\cdot(\theta_1-\theta_2)\cdot(T-t)\right]/T\Big]. \tag{25}$$

Here, θ represents the dynamic inertia weighting factor, where both θ_1 and θ_2 are weight parameters.

3.3.4 Lévy flight strategy

To prevent the northern goshawk from falling into the local optimal solution, which leads to premature convergence and failure to reach the optimal solution, the Lévy flight strategy is introduced in the second stage to the improve the performance of NGO. [24] The corresponding mathematical model is

$$\begin{cases}x_{i,j}^{P_2}(t+1)=x_{i,j}^{P_2}(t)+L\oplus L(\lambda)\\ L=0.01\cdot\left[x_{i,j}^{P_2}(t)-p_{i,j}(t)\right]\end{cases}. \tag{26}$$

Here, $\oplus$ is the point multiplication operation, L is the step control coefficient, and $L(\lambda)$ is the path function, which is usually simulated using the Mantegna algorithm. The method of setting the step size is

$$step=\alpha_1/\left|\alpha_2\right|^{1/\gamma}. \tag{27}$$

Here, γ is a constant and set to 1.5, α_1 and α_2 are random values that follow a normal distribution, and their variance is

$$\begin{cases}\alpha_1=\left\{\dfrac{\Gamma(1+\gamma)\cdot\sin(\pi\gamma/2)}{\gamma\cdot\Gamma\left[(1+\gamma)/2\right]\cdot 2^{(\gamma-1)/2}}\right\}\\ \alpha_2=1\end{cases}. \tag{28}$$

The flow of the improved algorithm is shown in Fig. 2.

4. Case Analysis

4.1 Basic data

An industrial park in northern China is taken as the research object, with 24 h as the operation cycle.[25] The model of IEHS that considers DR is built using MATLAB R2020a software.

4.2 Analysis of results

4.2.1 Comparative analysis of different scenarios of the same algorithm

In this paper, the INGO algorithm is selected for the comparative analysis of the following four different scenarios:
Scenario 1: Neither the carbon emission sensing measurement system nor DR are considered.
Scenario 2: Only the carbon emission sensing measurement system is considered.
Scenario 3: Only DR is considered.
Scenario 4: Both the carbon emission sensing measurement system and DR are considered.
The operation costs and carbon emissions of the four scenarios are shown in Table 1.

Table 1 shows that, in comparison with those of scenario 1, the carbon emission cost of scenario 2 is decreased by 53.9% and the actual carbon emission is diminished by 4884.543 kg. Compared with scenario 1, scenario 2, which considers the emission sensing measurement system, has reduced carbon emission and decreased operation costs. In comparison with that of scenario 1, the energy purchase cost of scenario 3 is reduced by 6.25%, which is due to the consideration of DR to reduce the peak load and increase the valley load. In comparison with those of scenarios 2 and 4, the total operation cost, carbon trading cost, and actual carbon emission of scenario 3 are high, which indicates the favorable effect of the carbon trading mechanism. The total operation cost, energy purchase cost, carbon trading cost, and actual carbon emission of scenario 4 are relatively small, which is due to the fact that considering DR

Table 1
Daily operation costs in four scenarios.

Case	Total operation cost (¥)	Energy purchase cost (¥)	Carbon trading cost (¥)	Actual carbon emission (kg)
1	20108.905	18383.754	1725.151	39664.194
2	18313.638	16674.573	795.267	34779.651
3	19181.408	17235.364	2088.530	37816.414
4	18017.079	16376.575	730.435	33243.612

within the carbon trading mechanism not only converts the peak load to a low load, but also achieves multi-energy compatibility and smooths the user load curve. In comparison with those of scenario 1, the total operation cost of scenario 4 is decreased by 10.4%, the energy purchase cost is reduced by 10.91%, the carbon emission cost is decreased by 57.66%, and the actual carbon emission is lessened by 6420.582 kg. Therefore, through the comparison of the four scenarios, scenario 4, in which the carbon emission sensing measurement system and DR are considered, is the most economical operation mode.

Figure 3 shows that the initial electricity price has been stable at 0.78 ¥/(kW·h) and the initial heat price at 0.37 ¥/(kW·h). After considering the time-of-use price, the electricity price is determined to be 1.09 ¥/(kW·h) in the peak period (10:00–12:00 and 20:00–22:00), 0.35 ¥/(kW·h) in the valley period (01:00–07:00 and 23:00–24:00), and 0.68 ¥/(kW·h) in the normal period (8:00–9:00 and 13:00–19:00). The peak and valley periods of heat and electricity prices are slightly different. The heat price is determined to be 0.58 ¥/(kW·h) in the peak period (11:00–14:00 and 20:00–22:00), 0.25 ¥/(kW·h) in the valley period (01:00–07:00 and 18:00–19:00), and 0.36 ¥/(kW·h) in the normal period (8:00–10:00 and 13:00–17:00). The user can change the interval of using electric and thermal energies in accordance with the price fluctuation, and the variation curve of electric and thermal loads is shown in Fig. 4.

Figure 4 shows that after considering DR, compared with the distribution of the original load, we achieved partial load reduction during high price periods and partial load transfer during low

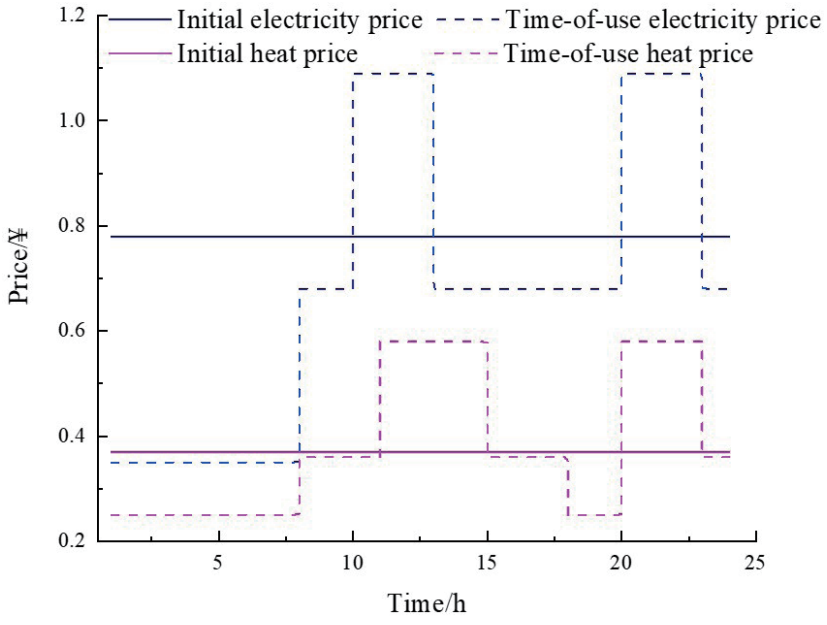

Fig. 3. (Color online) Price comparison diagram.

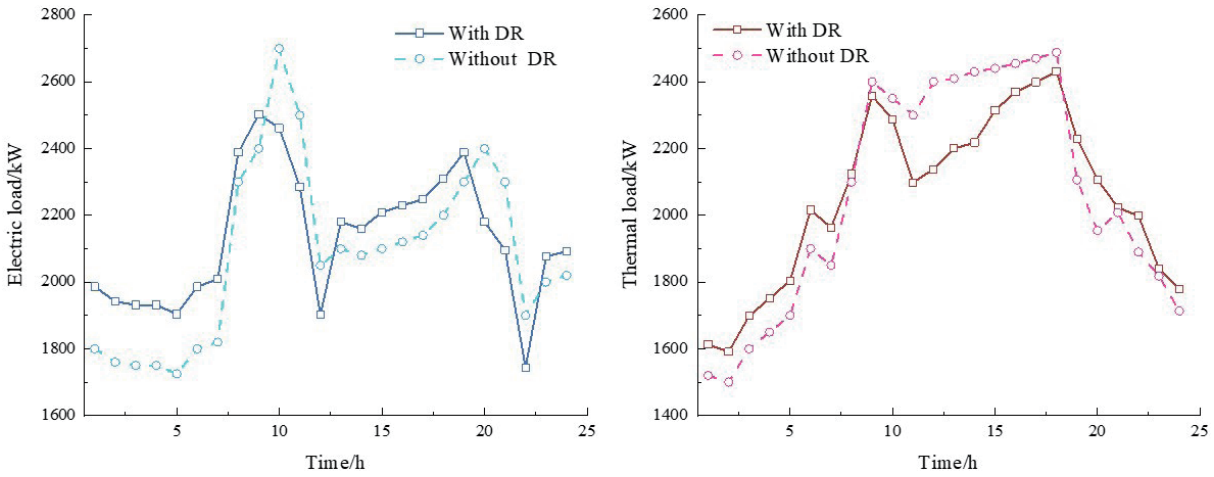

Fig. 4. (Color online) Load variation after considering DR.

price periods. The shiftable load transfer parts of the load during the periods of 09:00–12:00 and 19:00–22:00 are shifted to the periods of 23:00–07:00 and 13:00-18:00, rendering the load curve relatively smooth. The replaceable load converts part of the electric load into the thermal load during the high-electricity-price period and converts a portion of the thermal load into the electric load in the low-electricity-price period (11:00–19:00). Price- and replacement-based DRs work in synergy to realize peak shaving and valley filling.

4.2.2 Comparative analysis of different algorithms in same scenario

In scenario 4, four different algorithms, namely, PSO, SCA, NGO, and INGO, are compared and analyzed, as shown in Table 2.

Table 2 shows that, in comparison with those of the NGO algorithm, the total operation cost of the INGO algorithm is decreased by 9.4%, the energy purchase cost is decreased by 6.24%, the carbon trading cost is decreased by 17.53%, and the actual carbon emission is lessened by 1164.253 kg, which verifies the effectiveness of the INGO algorithm using the improved strategies and the improved performance of the algorithm overall. In scenario 4, the superiority and inferiority of different algorithms are ranked as INGO, NGO, PSO and SCA. Compared with those of SCA, the total operation cost of the INGO algorithm is decreased by 17.75%, the energy purchase cost is decreased by 17.09%, the carbon trading cost is decreased by 28.73%, and the actual carbon emission is decreased by 1917.411 kg. The performance of the original NGO is also better than those of PSO and SCA. The sine and cosine factor oscillation in SCA is introduced into the INGO algorithm, which further strengthens the performance of the INGO algorithm, and the results of its application in practical problems also prove this point. The

Table 2
Daily operation costs with four algorithms.

Algorithm	Total operation cost (¥)	Energy purchase cost (¥)	Carbon trading cost (¥)	Actual carbon emission (kg)
PSO	21904.832	19752.452	1024.849	35161.023
SCA	23497.658	21643.763	1198.371	36549.334
NGO	19886.524	17466.869	885.730	34407.865
INGO	18017.079	16376.575	730.435	33243.612

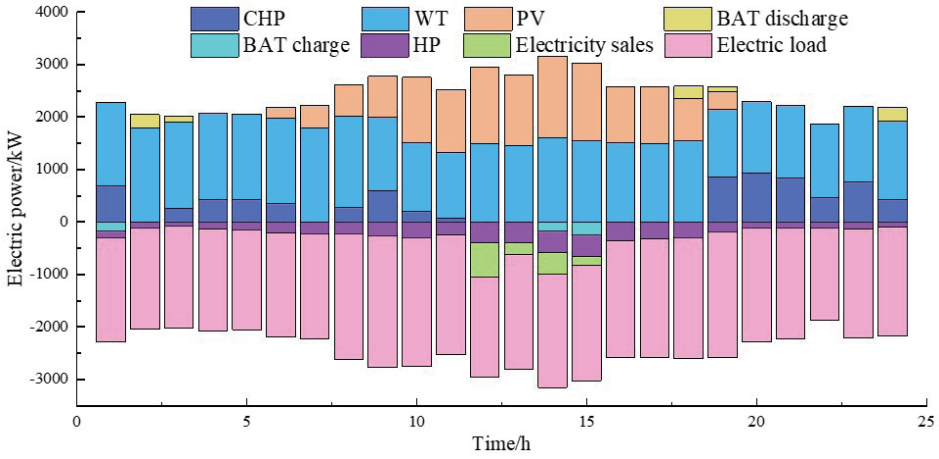

Fig. 5. (Color online) Electric power balance.

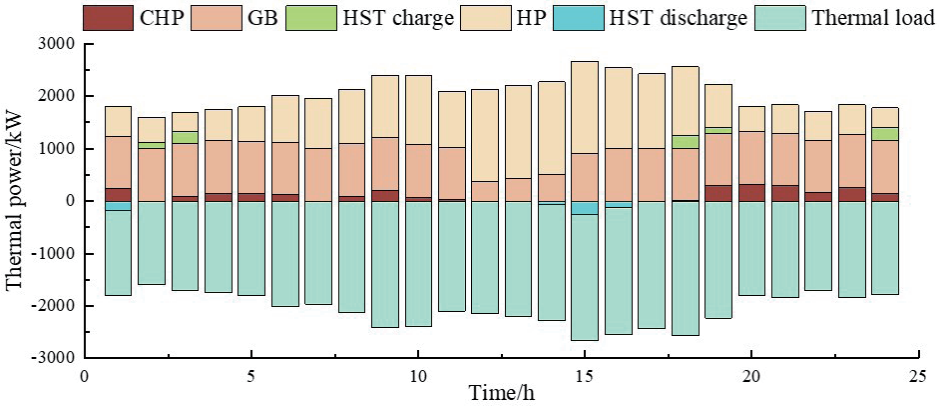

Fig. 6. (Color online) Thermal power balance.

INGO algorithm is far better than NGO and SCA in terms of convergence accuracy and also exceeds the classical intelligent algorithm PSO.

The electric and thermal power balances of the IEHS model solved by the INGO algorithm are shown in Figs. 5 and 6, respectively.

Figure 5 shows that, in the time period of 12:00–18:00, the output powers of PV and WT are relatively high. In the case of satisfying users' electric load and the HP of the electric equipment, part of the electric energy is stored by BAT and a portion of the electric energy is sold to the superior grid. In other time periods, when PV and WT fail to satisfy users' electric load, CHP and BAT supply and discharge power. Particularly in the time period when PV cannot supply power (20:00–5:00), CHP and WT are the main sources of power. At the same time, the electric load is also lower at night. The output of CHP is slightly smaller than that of WT, and the carbon emission generated will not be considerable. In the case of abundant electric energy, BAT will store the excess electric energy. In short, the strategy used to supply power to users is that PV and WT are preferentially utilized, followed by BAT discharge. If the electric load cannot be satisfied, CHP is finally utilized to maximize the use of electric energy. The consumed power of HP will vary with the change in users' thermal load. Compared with normal conditions, users consume more power during the peak period of heat load and less power during the trough period of heat load.

Figure 6 shows that the thermal load of users is less than the electric load, and the thermal power is mostly supplied by GB and HP. CHP also outputs a portion of the thermal power when providing electric power, and HST stores part of the thermal energy during the time when the thermal power is abundant (1:00 and14:00–16:00) and releases the thermal energy in the case of low carbon emission. Similarly to that of electric power, the supply of thermal power to the users' thermal demand follows the strategy of energy saving and emission reduction, with the priority HP supplying thermal load, followed by HST releasing thermal energy, and finally, GB and CHP outputting thermal energy to satisfy users when the thermal power supply is inadequate. This is due to the fact that compared with GB, HP consumes electric power to generate thermal power, which is more conducive to reducing carbon emission, especially at low electricity prices.

5. Conclusions

Aiming to realize IEHS, the authors established an economic dispatch model that incorporated the carbon emission sensing measurement system and DR, and proposed an INGO algorithm with superior performance. The results of different scenarios and algorithms are compared and analyzed, and the optimal dispatch scheme of the IEHS model is obtained. The results are as follows.

(1) After introducing the carbon emission sensing measurement system, the carbon emission cost is reduced by 53.9% and the actual carbon emission is reduced by 4884.543 kg, which achieves a low-carbon economic dispatch.
(2) After including DR, the energy purchase cost is reduced by 6.25%, which provides a financial energy purchase plan.
(3) With both the carbon emission sensing measurement system and DR, the total operation cost is decreased by 10.4%, the energy purchase cost is decreased by 10.91%, the carbon emission cost is reduced by 57.66%, and the actual carbon emission is decreased by 6420.582 kg.
(4) Compared with those of the NGO algorithm, the total operation cost of the INGO algorithm is reduced by 9.4% and the energy purchase and carbon trading costs are decreased by 6.24 and 17.53%, respectively, which verifies the practicability of the INGO algorithm.

Our main contributions are as follows. (1) An IEHS economic operation optimization model that incorporates the carbon emission sensing measurement system and DR is established. (2) An INGO algorithm that uses Bernoulli chaotic mapping, sine-cosine oscillation variation, dynamic inertia weighting factor, and Lévy flight strategy is introduced. (3) The effectiveness and practicability of the IEHS model and INGO algorithm are proved by the comparative analysis of different scenarios and algorithms.

Although we established an economic scheduling model, there is still room for improvement. Future research should focus on enhancing the coordinated operation efficiency among equipment, strengthening the coupling relationship of energy flow in the system, and reducing the loss during energy conversion and transmission. In addition, the effect of source-load uncertainty under DR needs to be further analyzed.

Acknowledgments

This study was supported by the “Chunhui Program” Collaborative Scientific Research Project of the Ministry of Education of the People's Republic of China (Project No. HZKY20220242) and the S&T Program of Hebei (Project No. 21567605H and No. 225676163GH).

References

1 J. X. Li, D. Wang, H. J. Jia, Y. Lei, T. S. Zhou, and Y. Guo: Appl. Energy **324** (2022) 119725. https://doi.org/10.1016/j.apenergy.2022.119725
2 T. F. Ma, J. Y. Wu, L. L. Hao, and D. Z. Li: Appl. Therm. Eng. **146** (2019) 648. https://doi.org/10.1016/j.applthermaleng.2018.10.022
3 Y. Liu, J. Zhao, L. Q. Wang, W. Wang: IEEE Trans. Ind. Electron. **70** (2023) 1005. https://doi.org/10.1109/TIE.2022.3152019
4 H. C. Chen, S. S. Li, and S. L. Wu: Sens. Mater. **34** (2020) 871. https://doi.org/10.18494/SAM3648

5 Z. Ni, S. Cai, and C. Ni: Sens. Mater. **35** (2023) 1835. https://doi.org/10.18494/SAM4310
6 Q. Zheng, Y. Gu, Y. Liu, J. Ma, and M. Peng: Electr. Power Syst. Res. **216** (2023) 108979. https://doi.org/10.1016/j.epsr.2022.108979
7 S. Yao, W. Gu, J. Wu, H. Lu, S. Zhang, and Y. Zhou: Appl. Energy **322** (2022) 108529. https://doi.org/10.1016/j.ijepes.2022.108529
8 B. Xu and Y. Xiang: Energy Rep. **8** (2022) 932. https://doi.org/10.1016/j.egyr.2022.08.066
9 Z. G. Deng, J. H. Yang, C. L. Dong, M. Q. Xiang, Y. Qin, and Y. S. Sun: Energy Rep. **8** (2022) 77. https://doi.org/10.1016/j.egyr.2022.03.072
10 C. Pan, H. Fan, R. Zhang, J. Sun, Y. Wang, and Y. Sun: Appl. Energy **343** (2023) 121137. https://doi.org/10.1016/j.apenergy.2023.121137
11 L. L. Li, X. Y. Ren, M. L. Tseng, D. S. Wu, and M. K. Lim: Energy Convers. Manag. **258** (2022) 115541. https://doi.org/10.1016/j.enconman.2022.115541
12 L. Kang, J. Wang, X. Yuan, Z. Cao, Y. Yang, and S. Deng: Energy Convers. Manag. **287** (2023) 117117. https://doi.org/10.1016/j.enconman.2023.117117
13 X. Li, T. Li, L. Liu, Z. Wang, X. Li, and J. Huang: J. Clean. Prod. **391** (2023) 136119. https://doi.org/10.1016/j.jclepro.2023.136119
14 Y. Zhu, Y. Xu, H. Chen, H. Guo, H. Zhang, and X. Zhou: Appl. Energy **343** (2023) 121113. https://doi.org/10.1016/j.apenergy.2023.121113
15 D. Yousri, H. E. Z. Farag, H. Zeineldin, and E. F. El-Saadany: Energy Convers. Manag. **280** (2023) 116809. https://doi.org/10.1016/j.enconman.2023.116809
16 K. Li, N. Ye, S. Li, H. Wang, and C. Zhang: Energy **273** (2023) 127137. https://doi.org/10.1016/j.energy.2023.127137
17 H. Ren, Z. Jiang, Q. Wu, Q. Li, and H. Lv: Energy **277** (2023) 127644. https://doi.org/10.1016/j.energy.2023.127644
18 X. Lyu, T. Liu, X. Liu, C. He, L. Nan, and H. Zeng: Energy **263** (2023) 125739. https://doi.org/10.1016/j.energy.2022.125739
19 L. L. Li, J. L. Lou, M. L. Tseng, M. K. Lim, and R. R. Tan: Expert Syst. Appl. **203** (2022) 117411. https://doi.org/10.1016/j.eswa.2022.117411
20 Z. F. Liu, L. L. Li, Y. W. Liu, J. Q. Liu, H. Y. Li, and Q. Shen: Energy **235** (2021) 121407. https://doi.org/10.1016/j.energy.2021.121407
21 M. Dehghani, S. Hubalovsky, and P. Trojovsky: IEEE Access **9** (2021) 162059. https://doi.org/10.1109/ACCESS.2021.3133286
22 L. L. Li, Z. F. Liu, M. L. Tseng, K. Jantarakolica, and M. K. Lim: Expert Syst. Appl. **184** (2021) 115579. https://doi.org/10.1016/j.eswa.2021.115579
23 S. R. Nayak, R. K. Khadanga, Y. Arya, S. Panda, and P. R. Sahu: Electr. Power Syst. Res. **223** (2023) 109513. https://doi.org/10.1016/j.epsr.2023.109513
24 H. T. Liang, and F. H. Kang: Optik **127** (2016) 8036. https://doi.org/10.1016/j.ijleo.2016.06.002
25 C. Wang, S. Jiao, Y. Li, and Q. Zhang: Expert Syst. Appl. **231** (2023) 120602. https://doi.org/10.1016/j.eswa.2023.120602

About the Authors

Ling-ling Li received her M.S. degree in control theory and control engineering in 2001 and her Ph.D. degree in electrical machinery and appliances in 2004 from Hebei University of Technology. She is currently a professor at the School of Electrical Engineering, Hebei University of Technology, and a permanent member of the State Key Laboratory of Reliability and Intelligence of Electrical Equipment. Her research interests include power systems, new energy, and electrical reliability. (lilingling@hebut.edu.cn)

Yan Miao received his B.S. degree in engineering from Taiyuan Institute of Technology in Taiyuan, Shanxi, China. He is currently pursuing his M.S. degree in electrical engineering from Hebei University of Technology. His research interests include hybrid smart grid optimization operation, renewable energy grid integration, and energy storage condition detection. (2021214011069@stu.hebut.edu.cn)

Cheng-Jian Lin received his B.S. degree in electrical engineering from Ta Tung Institute of Technology, Taipei, Taiwan, R.O.C., in 1986 and his M.S. and Ph.D. degrees in electrical and control engineering from National Chiao Tung University, Taiwan, R.O.C., in 1991 and 1996, respectively. Currently, he is a chair professor of the Department of Computer Science and Information Engineering, National Chin-Yi University of Technology, Taichung, Taiwan, R.O.C. His current research interests are in machine learning, pattern recognition, intelligent control, image processing, intelligent manufacturing, and evolutionary robots. (cjlin@ncut.edu.tw)

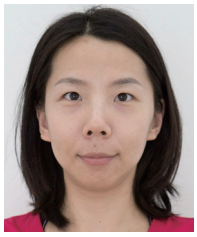

Li-nan Qu is a Ph.D. student at Hebei University of Technology and works in China Electric Power Research Institute, majoring in electric power system. Her main research fields include the modeling and simulation of renewable energy generation, model parameter identification, and the stability analysis of interconnected power systems. (201811401013@stu.hebut.edu.cn)

Guanchen Liu received his Ph.D. degree from Zhejiang University, Hangzhou, China, in 2020. Since 2021, he has been a postdoctoral student of Zhejiang University and has become a consultant of Power China Huadong Engineering Corporation Limited. His research interests include battery energy storage system, micro power systems, and control algorithms. (liu_gc3@hdec.com)

Jiaping Yuan received his B.Eng. degree in civil engineering from Zhejiang University, Hangzhou, China, in 2009. Since 2009, he has been with Power China Huadong Engineering Corporation Limited, where he is currently an advanced engineer, the President of the Electromechanical Engineering Institute, and the General Manager of Huachen Electric Power. His current major research interests include digital energy. (yuan_jp@hdec.co)